Communication: Phase Diagram of Ice Polymorphs under Negative Pressure Considering the Limits of Mechanical Stability

Takahiro Matsui,[1] Takuma Yagasaki,[2,a)] Masakazu Matsumoto,[2,b)] and Hideki Tanaka[2]

[1] *Graduate School of Natural Science and Technology, Okayama University, Okayama, 700-8530, Japan*

[2] *Research Institute for Interdisciplinary Science, Okayama University, Okayama, 700-8530, Japan*

Abstract

Thermodynamic and mechanical stabilities of various ultralow-density ices are examined using computer simulations to construct the phase diagram of ice under negative pressure. Some ultralow-density ices, which were predicted to be thermodynamically metastable under negative pressures on the basis of the quasi-harmonic approximation, can exist only in a narrow pressure range at very low temperatures because they are mechanically fragile due to the large distortion in the hydrogen bonding network. By contrast, relatively dense ices such as ice Ih and ice XVI withstands large negative pressure. Consequently, various ices appear one after another in the phase diagram. The phase diagram of ice under negative pressure exhibits a different complexity from that of positive pressure because of the mechanical instability.

Introduction

There are seventeen ice polymorphs.[1] Among them, ice XIII - XVII have been found in this century.[2–5] Ices XIII, XIV, and XV are hydrogen-ordered counterparts of ices V, XII, and VI, respectively.[2,3] By contrast, the molecular arrangements of ices XVI and XVII are different from that of any ice phase found earlier.[4,5]

Computer simulations have suggested new ice phases that are stable or metastable at extreme conditions such as negative pressure and very high pressure,[6–27] and several of them have been indeed synthesized in later experimental studies.[4,28,29] An example is empty sII clathrate hydrate. Simulation studies have shown that this structure is more stable than ice Ih in the deeply negative pressure region, P < -3000 bar.[16,21,22] It is quite difficult to maintain negative pressure experimentally. Instead, this ice structure, which was named ice XVI, was realized by vacuum pumping of Ne clathrate hydrate.[4] A similar technique was used to synthesize ice XVII from C0 hydrogen filled ice although the stability of this structure had not been predicted in simulation studies.[5]

The structure of ice XVI (i.e., empty sII hydrate) is isomorphic to that of MTN-type zeolite. It is possible to make an ice structure from a silica zeolite structure by removing oxygen, adding hydrogen so that the resultant structure follows the ice rule, and replacing silicon with oxygen.[30] The zeolite-based ice structures are less dense than that of ice Ih and can be candidates of stable ice phases in the negative pressure region. Many low-density ice structures have been explored on this basis.[19–21,30] It has been shown that ice structures of zeolite DOH,[21,30] RHO,[18] FAU,[17] ITT,[19] LTA, SOD, and AST[23] are relatively stable and may occupy regions in the phase diagram of ice under negative pressure (the DOH and SOD structures correspond to the structures of sH and sVII hydrates, respectively).

A structure of a type of zeolite can be regarded as a superstructure consisting of polyhedral nodes and prismatic pillar parts made of hydrogen bonded water molecules. In a previous paper, we demonstrated the possibility of designing artificial low-density ice structures by elongation of the pillar parts of the superstructure (Figure S1).[19] We call them *aeroice*.

The phase diagram of ice have been constructed theoretically on the basis of the thermodynamic stability, i.e., the Gibbs energy of the ice phases. The Gibbs energies have been calculated using the quasi-harmonic approximation[20] or the combination of the Einstein approach and the Gibbs-Duhem integration.[17,18] In both cases, it is assumed that the crystalline structure is maintained in the pressure and temperature region examined. There is no problem with this assumption at positive pressure because the Gibbs energy is mainly determined by the potential energy which is the origin of the stability of the lattice structure. By contrast, under negative pressure, the negative and large *PV* term can be a dominant part of the Gibbs energy. An extreme example is aeroice at the limit of elongation by adding the polygonal rings: its chemical potential (molar Gibbs energy) is negatively infinite because of the *PV* term while the potential energy is not so low. It would be thermodynamically metastable in that sense. However, such a structure must be mechanically unstable in the presence of thermal fluctuations and cannot exist for long time even if the Gibbs energy is very low.

In this study, we present a diagram of low-density ice phases under negative pressure in consideration of the mechanical instability. We demonstrate that a region of the thermodynamically most stable phase in the phase diagram is terminated by the limit of mechanical stability for all crystalline phases. The obtained diagram is much complicated than the usual phase diagram.

Methods

The phase diagram of water depends on the force field model[10,31] We employ the TIP4P/2005 force field model because it reproduces well the phase diagram for $0 < P < 1$ GPa.[32] This model has been used to construct the phase diagram under negative pressure in early studies.[17,21] Comparison with the phase diagrams obtained from different force fields, including quantum mechanical ones, is beyond the scope of this study although it is an important issue.

Figure S2 presents the potential energy of 200 zeolite-based ice structures plotted against the molar volume. The zeolite topologies are taken from the Database of Zeolite Structure web site which provides structural information on all of the zeolite framework types that have been approved by the Structure Commission of the International Zeolite Association.[33] Ice structures that have low potential energy and large molar volume can be stable phases under negative pressure. We select 16 such structures out of the 200 structures and calculate their Gibbs energies. All the selected structures are shown in Figures 1 and S3. We also calculate the Gibbs energies of the *dtc* structure[34,35] and three aeroices.[19] The dtc structure is a hypothetical zeolite structure which is similar to ITT (Figure 1). The aeroice structures, *n*xFAU with $n = 2$, 3, and 4, are obtained by elongation of the pillar parts of the FAU structure, where n is the number of the repetitions of the pillar. The GenIce tool is used to generate all ice structures.[36] We only consider hydrogen disordered structures because it is difficult to determine the most stable hydrogen-ordered configuration uniquely for each ice type (there are 16 possible configurations even for the simple ice Ih structure).[37] The pillar part of the three aeroices is an exception: this part was found to be stable only with a specific hydrogen ordered configuration.[19]

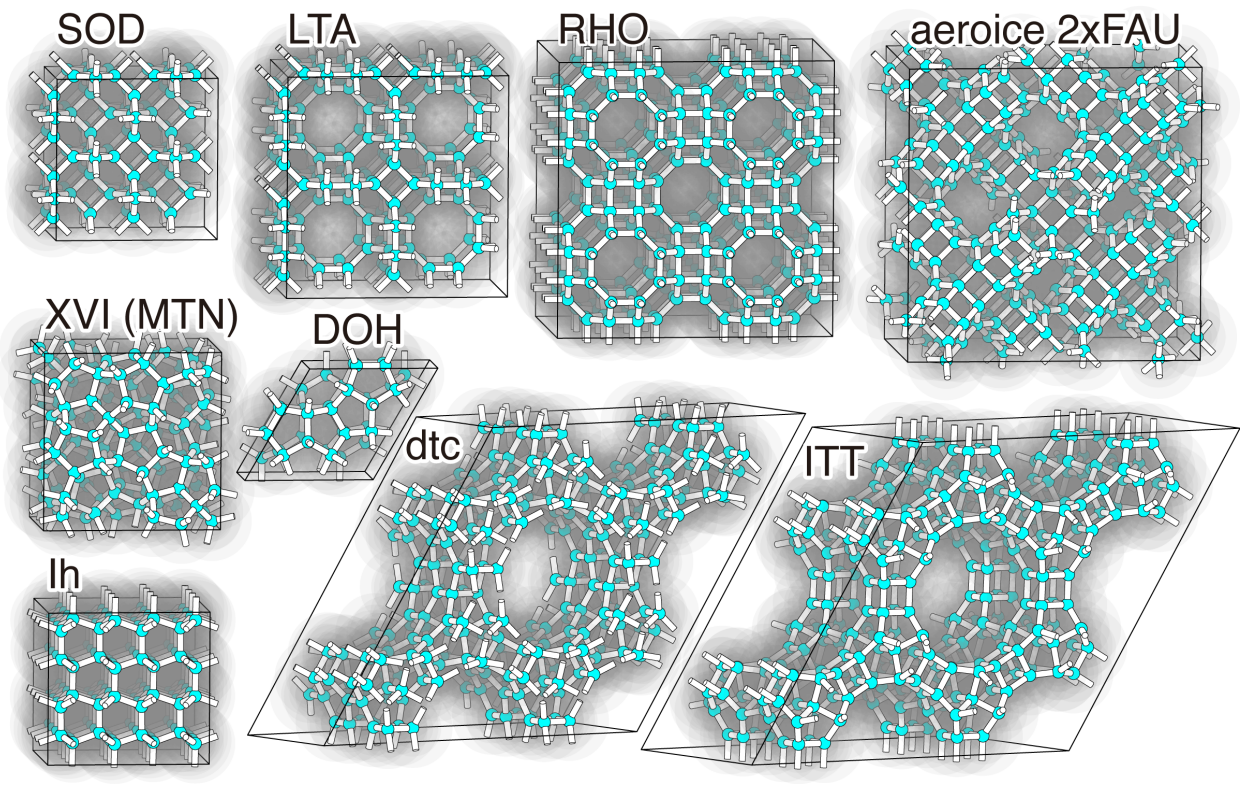

Figure 1. Structures of ices appeared in the phase diagram under negative pressure.

The Gibbs energy is calculated using the quasi-harmonic approximation with a homemade program code.[38] In this method, the Helmholtz energy of an ice structure is expressed as the sum of the potential energy at 0 K, the harmonic vibrational energy and entropy at given temperature derived from normal mode frequencies, and the Pauling entropy. The Gibbs energy is obtained from minimization of the Helmholtz energy at given pressure and temperature.

Molecular dynamics simulations are performed using the GROMACS 4.6 package to evaluate the mechanical stability of low-density ice structures.[39,40] We define that the ice structure is mechanically unstable when it dissociates within 10 ns in the MD simulation. The temperature is kept at either 50, 100, 150, 200, or 250 K using a Nosé-Hoover thermostat.[41,42] The pressure is

maintained by a Berendsen barostat.[43] The pressure is scanned in a range from -16 kbar to 0 kbar with an interval of 0.5 kbar. The liquid phase is not considered in this study because the Gibbs energy of ice Ih is lower than that of the liquid phase for TIP4P/2005 water at all the thermodynamic conditions.[44]

Results and Discussion

Figure 2a shows the Gibbs energies of ices MTN, DOH, and LTA at 250 K relative to that of ice Ih. Ice Ih is the most stable phase at P = 0 bar. Ice MTN becomes more stable than ice Ih for P < -2.5 kbar and ice LTA becomes the most stable phase for P < -3.8 kbar. The Gibbs energy of either of these three structures are lower than that of the other structures examined in this study at this temperature.

As shown in Figure 1, LTA is ultralow-density ice with large cavities. The Gibbs energy of this structure is quite low at deeply negative pressures because of the PV term under the quasi-harmonic approximation. However, it is expected that this structure, which contains four-membered rings of hydrogen bonding, cannot sustain for a long time in the deeply negative pressure region where the lattice structure is strongly stretched. The dashed lines in Figure 2b indicate the mechanically unstable regions evaluated using the MD simulations. The LTA structure dissociates quickly at pressures lower than -4.0 kbar. This means that LTA ice exists as the most stable phase only in the very narrow pressure range, -4.0 < P < -3.8 kbar. Because of the mechanical disruption, MTN ice again becomes the most stable for P < -4.0 kbar. The phase transition from MTN to DOH occurs at P = -5 kbar but the DOH structure cannot be mechanically stable for P < -7 kbar. As a result, MTN ice thrice appears as the most stable phase.

Figure 2c shows the phase diagram considering the limit of mechanical stability. For P < -9 kbar, even ice Ih dissociates. No crystalline structure can exist in this region.

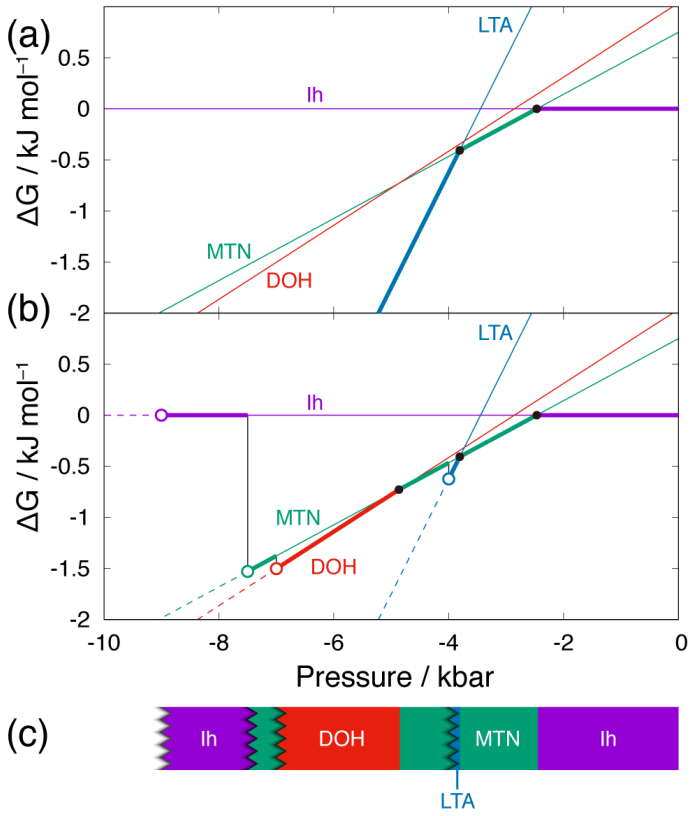

Figure 2.

(a) Gibbs energies of ices MTN, DOH, and LTA relative to that of ice Ih at 250 K. A black filled circle indicates a phase boundary where the Gibbs energies of two phases become the same. The thick lines constituting the lower envelope indicate the thermodynamically most stable phases among all ice phases. DOH cannot be the most stable phase at any pressure.

(b) An open circle shows a limit of mechanical stability dividing the mechanically stable (solid) and unstable (dashed) regions. The thick lines indicate the thermodynamically most stable phases among mechanically stable ice phases.

(c) Phase diagram of ice polymorphs at 250 K under negative pressure considering the limits of mechanical stability represented by zigzag lines. The pressure of the limit may increase when the threshold for the mechanical stability is longer than the present value of 10 ns.

The phase behavior at 50, 100, 150, 200, and 250 K are summarized in Figure 3. The Gibbs energies of ice phases used to obtain the diagram are given in Figure S4. Simulation studies of Conde et al., Jacobson et al., and Huang et al. suggested that a wide area of the diagram is occupied by MTN (empty sII hydrate).[17,18,21,22] In our diagram, the area of MTN is narrow because of ice dtc which has not been considered in the previous studies. There exists a large area of DOH (empty sH hydrate). This is consistent with the result of TIP4P/2005 water reported by Conde et al.[21] Ultralow-density ice ITT and aeroices 2xFAU, 3xFAU, and 4xFAU are thermodynamically metastable at very low temperatures but are mechanically very fragile and therefore they occupy only very narrow pressure ranges. Other ultralow-density ices which are not considered in this study, such as FAU aeroice with $n > 4$, would also occupy very narrow ranges and the presence of such phases tessellate the diagram into many pieces at temperatures lower than 50 K. If the hydrogen order-disorder transitions are taken into account, it would be further tessellated.

The density of ice Ih is the highest among those of all other ices considered in the present study. Therefore, ice Ih appears as the thermodynamically most stable phase in the high pressure region of the diagram irrespective of temperature. On the other hand, ice Ih is the mechanically most stable because of the least distortion in the network structure. Therefore, ice Ih always

occupies the lowest-pressure region of the diagram. This reentrance is characteristic for the phase behavior under negative pressure.

Ice structures including many four-membered rings are mechanically unstable. (Table S1) We define the ratio of the number of *n*-membered rings to the number of hydrogen bonds as p_n. Ice Ih consists only of 6-membered rings and ice XVI (MTN) consists of 5- and 6-membered rings, so their p_4 values are 0. These two ices are indeed mechanically stable under deeply negative pressure. DOH and dtc, whose p_4 are 4% and 15%, respectively, are also not so weak against mechanical stretching. An ice structure with a small p_4 value is stable thermodynamically as well as mechanically. Therefore, the phase diagram under negative pressure is dominated by the four ices, Ih, XVI, DOH, and dtc. The ITT (p_3>0), LTA, RHO (p_4=38%), and aeroice (p_4>40%) structures are fragile because of the abundance of four-membered rings and even less stable three-membered rings.

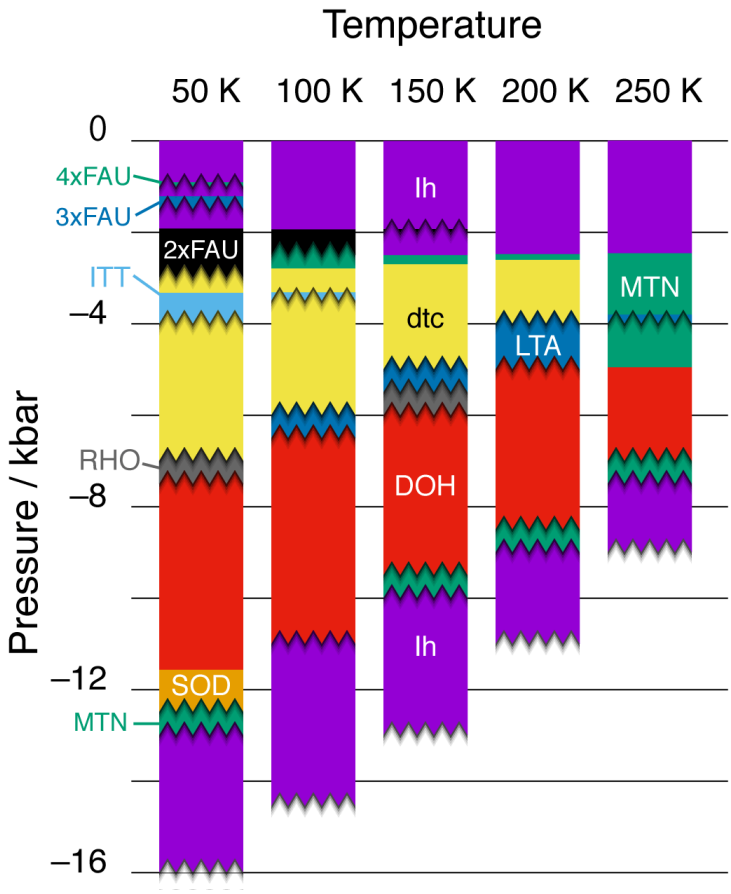

Figure 3. Phase diagram of TIP4P/2005 under negative pressure considering mechanical stability.

Conclusions

We present a phase diagram of ice polymorphs under negative pressure in consideration of mechanical stability. The Gibbs energies of low-density ice phases are calculated under the quasi-harmonic approximation and the mechanical stabilities are evaluated using molecular dynamics simulations. Mechanically fragile ultralow-density ice structures that contain many four-membered rings can exist only in very narrow pressure ranges under negative pressure

although they are assessed to be thermodynamically metastable because of the *PV* term in the Gibbs energy. As a result, the phase diagram is tessellated into many parts especially at very low temperatures. Ice Ih and ice XVI, which do not contain unstable four-membered rings, appear in the phase diagram near 0 bar and in the deeply negative pressure region as thermodynamically metastable phases and as mechanically stable phases, respectively. This reentrance is characteristic for the phase behavior under negative pressure.

It may seem odd to think of fictitious negative pressure ices that are currently far from experimentally accessible. However, it must be noted that it took more than 10 years to obtain ice XVI experimentally since its presence was first predicted from computer simulations.[4,16] It is possible that there exist routes to form ultra-low density ice phases via solid-solid phase transitions under some conditions although the resultant phases might dissociate quickly because of the mechanical or thermodynamic instability. Molecular dynamics simulations may help to discover such routes because it allows to trace short-lived states under well-controlled extreme conditions.

Author Information

a) Electronic mail: t.yagasaki@gmail.com

b) Electronic mail: vitroid@gmail.com

Acknowledgments

The present work was supported by a grant of MORINO FOUNDATION FOR MOLECULAR SCIENCE and JSPS KAKENHI Grant No. 16K05658 and MEXT as “Priority

Issue on Post-Kcomputer" (Development of new fundamental technologies for high-efficiency energy creation, conversion/storage and use).

References

[1] V.F. Petrenko and R.W. Whitworth, *Physics of Ice* (2002).

[2] C.G. Salzmann, P.G. Radaelli, A. Hallbrucker, E. Mayer, and J.L. Finney, Science **311**, 1758 (2006).

[3] C.G. Salzmann, P.G. Radaelli, E. Mayer, and J.L. Finney, Phys. Rev. Lett. **103**, 105701 (2009).

[4] A. Falenty, T.C. Hansen, and W.F. Kuhs, Nature **516**, 231 (2014).

[5] L. Del Rosso, M. Celli, and L. Ulivi, Nat. Commun. **7**, 13394 (2016).

[6] Y. Takii, K. Koga, and H. Tanaka, J. Chem. Phys. **128**, 204501 (2008).

[7] K. Himoto, M. Matsumoto, and H. Tanaka, Phys. Chem. Chem. Phys. **16**, 5081 (2014).

[8] M. Hirata, T. Yagasaki, M. Matsumoto, and H. Tanaka, Langmuir **33**, 11561 (2017).

[9] K. Mochizuki, K. Himoto, and M. Matsumoto, Phys. Chem. Chem. Phys. **16**, 16419 (2014).

[10] T. Yagasaki, M. Matsumoto, and H. Tanaka, J. Phys. Chem. B **122**, 7718 (2018).

[11] J. Russo, F. Romano, and H. Tanaka, Nat. Mater. **13**, 733 (2014).

[12] C.J. Fennell and J. Daniel Gezelter, J. Chem. Theory Comput. **1**, 662 (2005).

[13] T. Nakamura, M. Matsumoto, T. Yagasaki, and H. Tanaka, J. Phys. Chem. B **120**, 1843 (2015).

[14] S. Pipolo, M. Salanne, G. Ferlat, S. Klotz, A.M. Saitta, and F. Pietrucci, Phys. Rev. Lett. **119**, 245701 (2017).

[15] J.L. Aragones, M.M. Conde, E.G. Noya, and C. Vega, Phys. Chem. Chem. Phys. **11**, 543 (2009).

[16] V.I. Kosyakov and V.A. Shestakov, Dokl. Phys. Chem. **376**, 49 (2001).

[17] Y. Huang, C. Zhu, L. Wang, J. Zhao, and X.C. Zeng, Chem. Phys. Lett. **671**, 186 (2017).

[18] Y. Huang, C. Zhu, L. Wang, X. Cao, Y. Su, X. Jiang, S. Meng, J. Zhao, and X.C. Zeng, Sci Adv **2**, e1501010 (2016).

[19] T. Matsui, M. Hirata, T. Yagasaki, M. Matsumoto, and H. Tanaka, J. Chem. Phys. **147**, 091101 (2017).

[20] E.A. Engel, A. Anelli, M. Ceriotti, C.J. Pickard, and R.J. Needs, Nat. Commun. **9**, 2173 (2018).

[21] M.M. Conde, C. Vega, G.A. Tribello, and B. Slater, J. Chem. Phys. **131**, 034510 (2009).

[22] L.C. Jacobson, W. Hujo, and V. Molinero, J. Phys. Chem. B **113**, 10298 (2009).

[23] Y. Liu and L. Ojamäe, Phys. Chem. Chem. Phys. **20**, 8333 (2018).

[24] I.M. Svishchev and P.G. Kusalik, Phys. Rev. B: Condens. Matter Mater. Phys. **53**, R8815 (1996).

[25] J.-A. Hernandez and R. Caracas, J. Chem. Phys. **148**, 214501 (2018).

[26] M. Benoit, M. Bernasconi, P. Focher, and M. Parrinello, Phys. Rev. Lett. **76**, 2934 (1996).

[27] B. Militzer and H.F. Wilson, Phys. Rev. Lett. **105**, 195701 (2010).

[28] P.C. Myint and J.L. Belof, J. Phys. Condens. Matter **30**, 233002 (2018).

[29] S. Klotz, K. Komatsu, F. Pietrucci, H. Kagi, A.-A. Ludl, S. Machida, T. Hattori, A. Sano-Furukawa, and L.E. Bove, Sci. Rep. **6**, 32040 (2016).

[30] G.A. Tribello, B. Slater, M.A. Zwijnenburg, and R.G. Bell, Phys. Chem. Chem. Phys. **12**, 8597 (2010).

[31] E. Sanz, C. Vega, J. L. F. Abascal, and L. G. MacDowell, Phys. Rev. Lett. 92, 255701 (2004).

[32] J.L.F. Abascal and C. Vega, J. Chem. Phys. **123**, 234505 (2005).

[33] C. Baerlocher, L.B. McCusker, and D.H. Olson, *Atlas of Zeolite Framework Types* (Elsevier, 2007).

[34] O.D. Friedrichs, A.W.M. Dress, D.H. Huson, J. Klinowski, and A.L. Mackay, Nature **400**, 644 (1999).

[35] M. O'Keeffe, M.A. Peskov, S.J. Ramsden, and O.M. Yaghi, Acc. Chem. Res. **41**, 1782 (2008).

[36] M. Matsumoto, T. Yagasaki, and H. Tanaka, J. Comput. Chem. **39**, 61 (2018).

[37] S. Singer, J.-L. Kuo, T. Hirsch, C. Knight, L. Ojamäe, and M. Klein, Phys. Rev. Lett. **2005**, *94* (13), 135701.

[38] Y. Koyama, H. Tanaka, G. Gao, and X.C. Zeng, J. Chem. Phys. **121**, 7926 (2004).

[39] D. Van Der Spoel, E. Lindahl, B. Hess, G. Groenhof, A.E. Mark, and H.J.C. Berendsen, J. Comput. Chem. **26**, 1701 (2005).

[40] B. Hess, C. Kutzner, D. van der Spoel, and E. Lindahl, J. Chem. Theory Comput. **4**, 435 (2008).

[41] S. Nosé, J. Chem. Phys. **81**, 511 (1984).

[42] W.G. Hoover, Phys. Rev. A Gen. Phys. **31**, 1695 (1985).

[43] H.J.C. Berendsen, J.P.M. Postma, W.F. van Gunsteren, A. DiNola, and J.R. Haak, J. Chem. Phys. **81**, 3684 (1984).

[44] M.M. Conde, M. Rovere, and P. Gallo, J. Chem. Phys. **147**, 244506 (2017).